Electronic Supplementary Material (ESI) for Lab on a Chip.
This journal is © The Royal Society of Chemistry 2021

Supplementary Information

Rapid quantitative assays for glucose-6-phosphate dehydrogenase (G6PD) and hemoglobin combined on a capillary-driven microfluidic chip

Marco Rocca[a,b], Yuksel Temiz[a], Marie L. Salva[a,b], Samuel Castonguay[c], Thomas Gervais[c,d,e], Christof M. Niemeyer[b], Emmanuel Delamarche*[a]

[a]IBM Research Europe - Zurich, 8803 Rüschlikon, Switzerland; [b]Karlsruhe Institute of Technology (KIT) – Institute for Biological Interfaces (IBG-1), 76344 Eggenstein-Leopoldshafen, Germany; [c]Department of Engineering Physics, Polytechnique Montréal, Montréal, Québec, Canada; [d]Institut du Cancer de Montréal, Montréal, Québec, Canada; [e]Centre de Recherche du Centre Hospitalier de l'Université de Montréal (CRCHUM), Montréal, Québec, Canada

* Emmanuel Delamarche

Email: emd@zurich.ibm.com

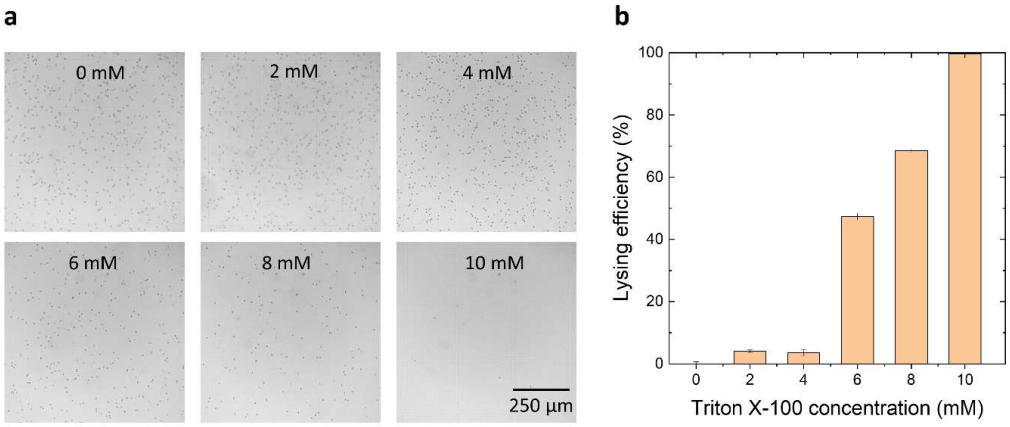

Fig. S1. RBC lysis using Triton X-100.[1] (a) Microscope images of RBCs on a cell counter after lysis using different Triton X-100 concentrations and diluting the samples 1:1000 in PBS to facilitate cell counting. The desired amount of whole blood was added to an Eppendorf tube containing a specific amount of Triton X-100. For this, 10 µL of 10 mM Triton X-100 in PBS was pipetted into the Eppendorf tube and the solution was allowed to evaporate under ambient conditions. Then a precise volume of whole blood (10 µL up to 100 µL) was added to obtain Triton X-100 concentrations between 10 and 1 mM. (b) Statistical analysis of the lysis efficiency as a function of Triton X-100 concentration. A concentration of 10 mM Triton X-100 was found to be sufficient to fully lyse RBCs within 3 minutes. All experiments were performed in duplicates and the error bars represent the standard deviation.

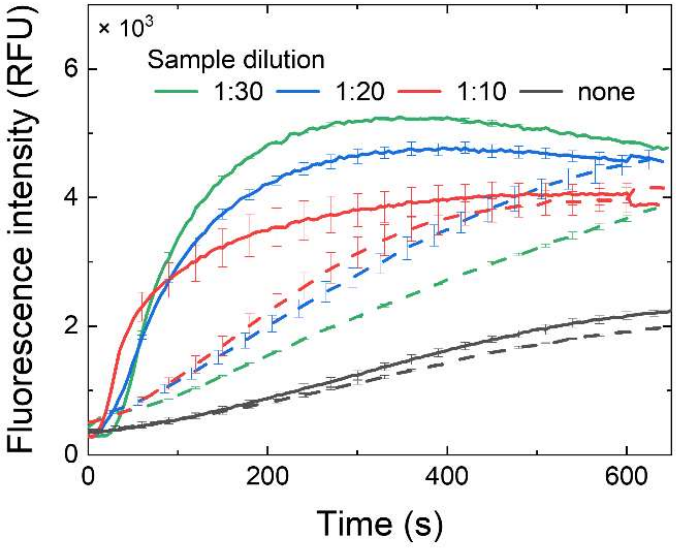

Fig. S2. Effect of dilution of whole blood samples with 20 mM Tris buffer on the generation of resorufin in a G6PD assay performed on a microfluidic chip. Plain curves correspond to blood spiked with 1000 µU/µL G6PD post-dilution. Dashed lines are negative controls (no spiked G6PD) with their slopes indicating the generation of fluorescent product during the coupled enzymatic reaction due to the activity of some G6PD in whole blood. The error bars represent the standard deviation. The fluorescence intensity is expressed in relative fluorescence units (RFU). The smaller slope in the black curves (no dilution) compared to the other curves might be related to the oxidation of NADPH back to NADP+ (e.g. by the enzyme glutathione reductase). This process will compete with diaphorase for NADPH and hence less resazurin will be reduced to resorufin. Diluting the sample reduces the concentration of glutathione reductase and this would explain why a dilution step results in an increase in the fluorescence signal.

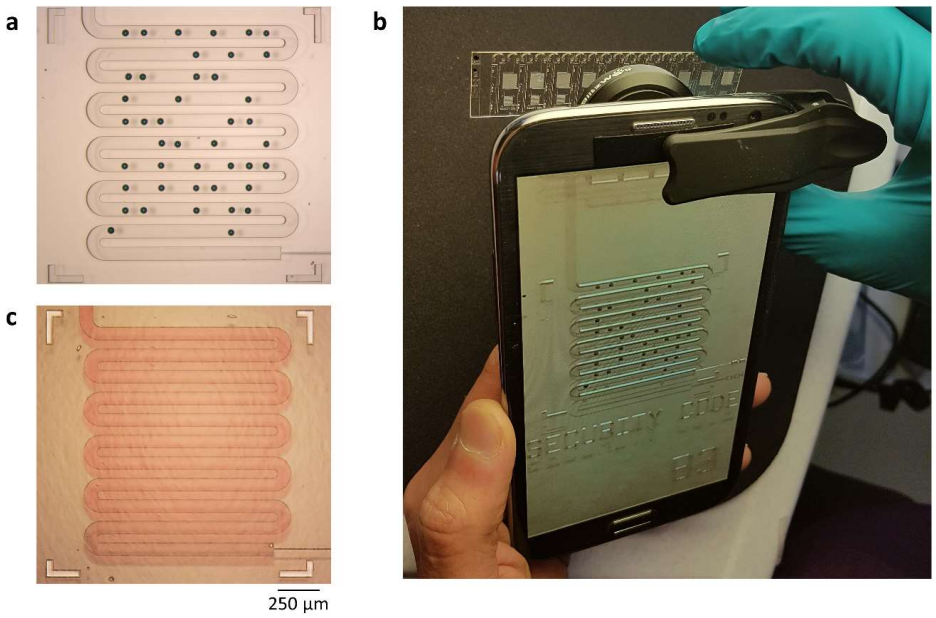

Fig. S3. Optical security code. (a) Micrograph of a pseudo-random generated security code created by inkjet spotting dyes in a microfluidic channel located after the hemoglobin measurement area. (b) The security code can be imaged using a smartphone equipped with a macro lens for identification/authentication of a microfluidic chip. (c) The security code is erased by the sample when the flow path is filled. The security level of the optical code can be enhanced for example by using dyes with multiple colors and/or adding soluble and insoluble dyes.[2]

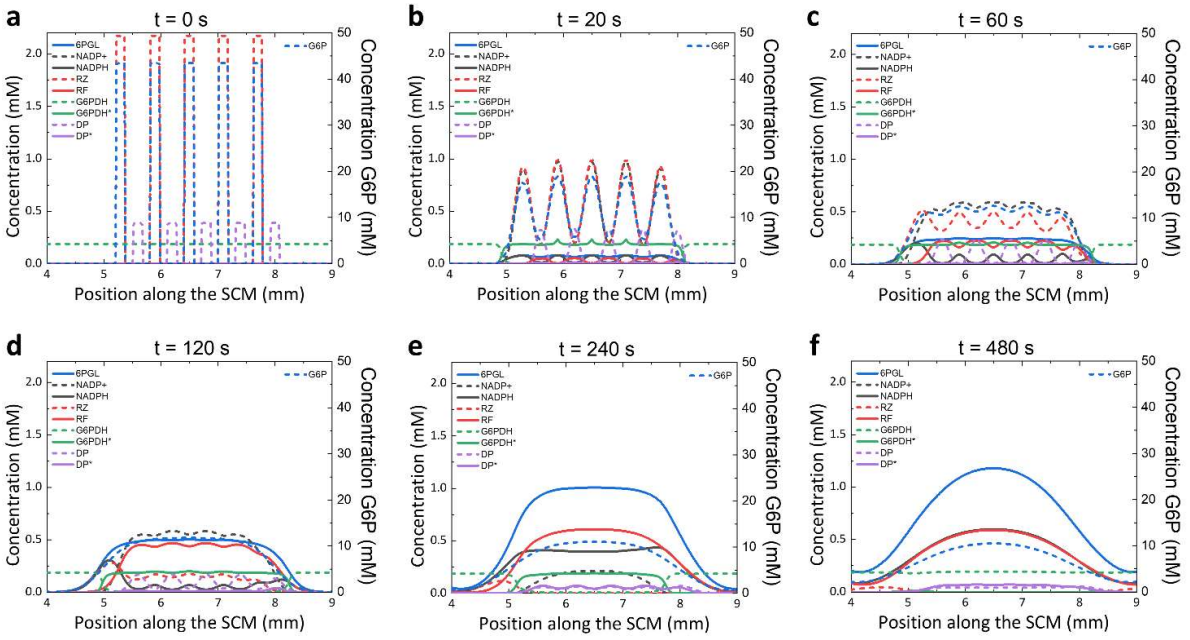

Fig. S4. Numerical simulation showing the evolution of the concentration of the reagents involved in the G6PD assay over the SCM length (*x* axis) for multiple time points. Dashed lines represent the evolution of the reagents spotted initially. Solid lines represent the reagents generated during the coupled enzymatic reactions. G6PD* and DP* indicate the activated state of the enzymes, when the cofactor is bound to the enzyme. Fluorescent resorufin, the measured product, is represented by the solid red curve. Note that the concentration of G6P is displayed on the right y-axis using a different scale.

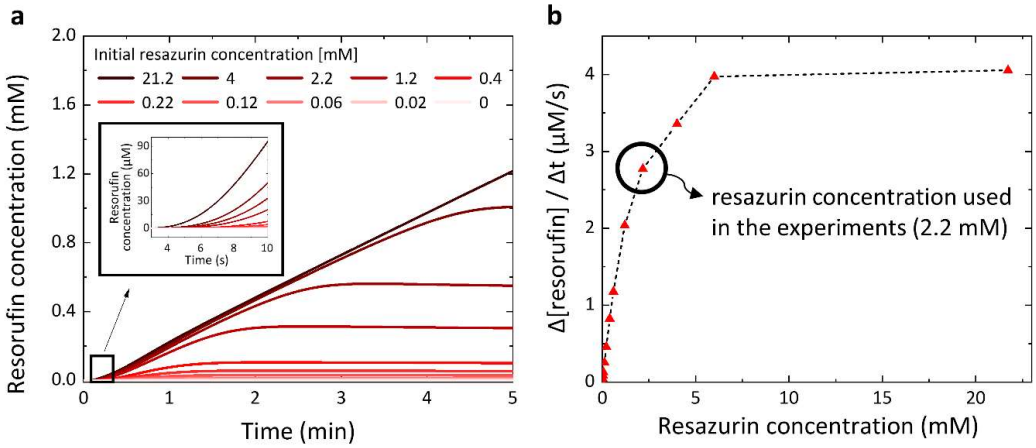

Fig. S5. Numerical simulation of the G6PD assay with varying initial concentration of the substrate resazurin. (a) For a higher initial concentration of resazurin the plateau in the assay kinetics increases and is reached at a later point in time. The inset is a zoom of the first 10 s of the assay kinetic and shows that the numerical model can predict the initial parabolic increase in the generation of resorufin (in accordance with experimental evidence shown in Fig 3*A*. (b) Slope of the kinetic curve plotted against the initial concentration of resazurin. This Michaelis-Menten-like graph provides a guideline for the initial concentration of resazurin to be used. Ideally, for enzyme activity measurements, the substrate concentration should be located in the plateau region. This result suggests that the initial concentration of resazurin should be increased in order to optimize the measurement of the enzymatic activity.

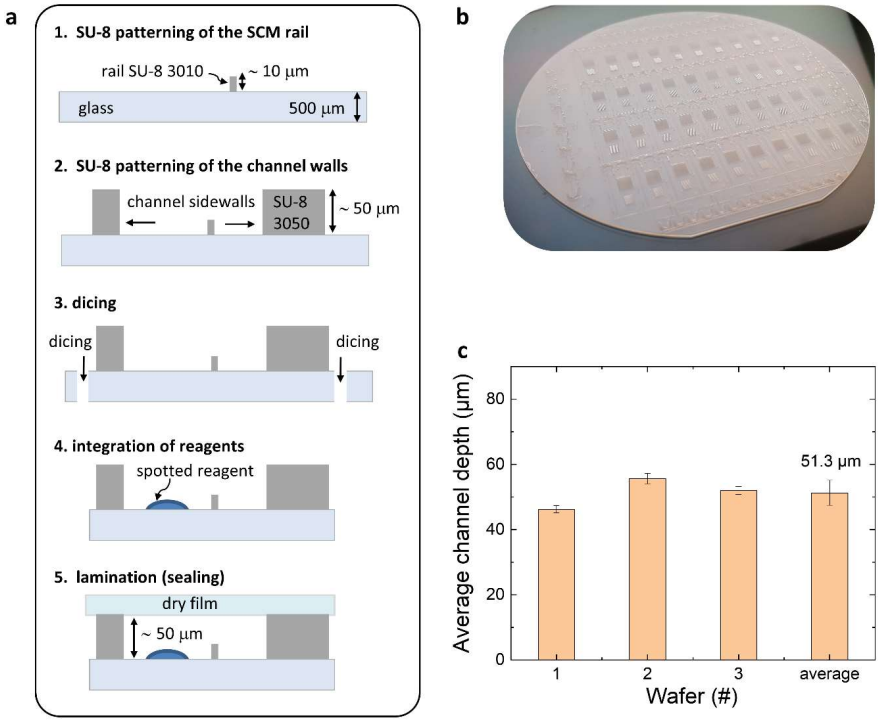

Fig. S6. Fabrication process of the microfluidic chips using 4" glass wafers. (a) Cross-sectional illustration of the wafer-level fabrication process involving photolithographic patterning of two SU-8 layers, wafer dicing, reagent integration and chip lamination. A dry film resist is used for chip lamination at this prototyping stage as it is a convenient method for sealing chips without interference from particulates and can be easily performed both on a single chip level or on a wafer level. (b) Picture of a 4" glass wafer with 40 microfluidic chips. (c) Microfluidic channel depth variation measured across 3 wafers. The largest variation in channel depth among all the performed measurements is 14.42%. The error bars represent the standard deviation.

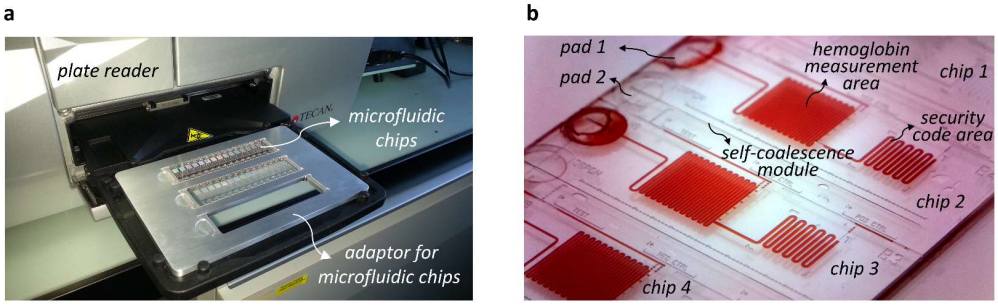

Fig. S7. (a) Setup for accommodating microfluidic chips on a microtiter plate reader for G6PD fluorescence and hemoglobin absorbance assays. A custom-made milled aluminum adaptor can hold multiple microfluidic chips for insertion into the reader. For measuring assays, only 3 chips were loaded with a sample and measured simultaneously, which overall took 2 minutes (the first 2 minutes of the assay kinetics are sufficient). Therefore, on average, 3 samples can be expected to be measured every few minutes. (b) Photograph showing microfluidic chips filled with blood by capillary forces and before insertion into the reader. Blood in pad 2 and the flow path (e.g. SCM) for the G6PD assay is not well visible due to dilution.

Movie S1. Filling of the capillary pump with a lysed whole blood sample by capillarity for performing an absorbance measurement of hemoglobin. The lysate gradually fills a capillary pump. The pinning features in the capillary pump avoid trapping air, which might affect the absorbance measurement. Multiple air vents at the end of the capillary pump ensure that no air bubbles get trapped.

Movie S2. Filling of the SCM by capillarity with a sample with a known G6PD concentration diluted in the assay buffer for performing the G6PD assay, negative and positive controls. The liquid gets pinned by the capillary pinning feature and is guided till the end of the module (from left to right). The interruption of the capillary pinning feature allows the meniscus to collapse and trigger a self-coalescing flow. The direction of the flow is dominated by the vertical component (orthogonal to the main axis of the SCM) and hence there is only minimal dragging of the reagents along the main axis of the SCM.

Mathematical modeling of resorufin production from two enzyme reaction cascade

1) Enzymatic reaction model

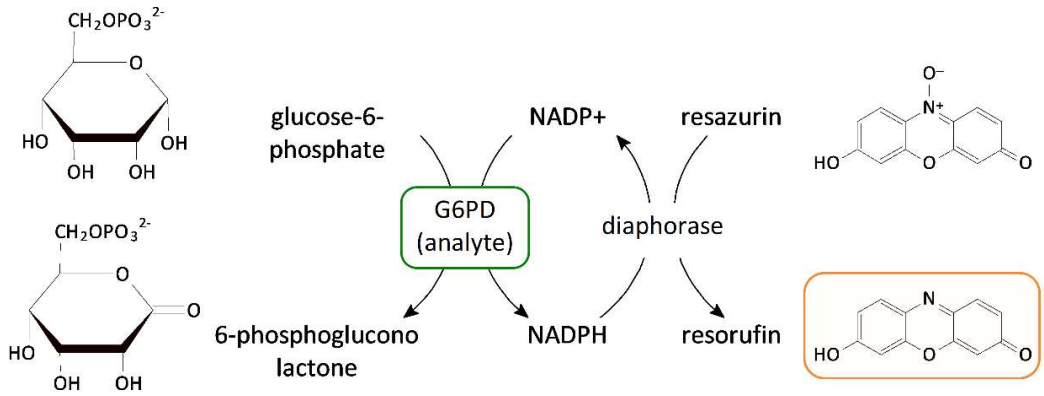

Fig. S8. Coupled enzymatic reactions relating the activity of G6PD to the reduction of resazurin to the fluorescent product resorufin. This highlights the role of the coupling factor $NADP^+$-NADPH in converting G6PD activity to fluorescence signal.

The conversion of resazurin (RZ) into fluorescent resorufin (RF*) by the enzyme diaphorase (DP) requires NADPH, which is provided from the reduction of $NADP^+$ during the conversion of glucose-6-phosphate (G6P) into 6-phosphogluconolactone (6PGL) by the enzyme glucose-6-phosphate dehydrogenase (G6PD).
Initially, G6P, $NADP^+$, RZ, and diaphorase and DP are spotted into the system and dried. The enzyme G6PD is brought in with the reconstitution buffer and the reaction starts.

Table S1. List of abbreviations and variable definition used for the mathematical model

Variable	Initial value	Definition
G6PD	0	Enzyme which needs to be quantified in the assay
G6PD*	0	Activated G6PD (when $NADP^+$ is bound to the enzyme)
DP	[DP]_0	Diaphorase enzyme
DP*	0	Activated Diaphorase (when NADPH is bound to the enzyme, produces fluorescence)
G6P	[G6P]_0	Glucose-6-phosphate, substrate of G6PD enzyme
6PGL	0	6-phosphogluconolactone (product of G6P conversion, inert)
RZ	[RZ]_0	Resazurin, fluorescence precursor and substrate of diaphorase
RF*	0	Resorufin, fluorescent molecule, product of RZ conversion by diaphorase
NADPH	0	Cofactor binding to diaphorase, product of G6PD G6P conversion
$NADP^+$	[$NADP^+$]_0	Cofactor binding to G6PD, product of DP RZ conversion

2) Reaction equations

The following reaction equations couple the different products together:

i) $G6P + NADP^+ + G6PD \rightleftharpoons 6PGL + NADPH + G6PD + H^+$ (2.1)
ii) $RZ + DP + NADPH \rightleftharpoons RF^* + NADP^+ + DP + H^+$ (2.2)

3) Model statement and assumptions

Based on this model, we will now proceed to state a certain number of assumptions and approximations. Assumptions are logical steps taken given the body of knowledge in the field. They can be considered exact or very strong as they stem from first principle models and solid knowledge from the literature. Approximations, on the other hand, are steps taken to simplify the problem, incurring an "exactness penalty". These approximations will be validated using the data obtained and presented later.

First assumption: Infinitely slow reactions in the absence of enzymes
A1) In the absence of enzyme, we will suppose these reactions infinitely slow (not occurring) and, as such, only the catalyzed reaction will generate products and these products will accumulate indefinitely. (unless, like NADPH, they are converted back by another enzymatic reaction)

Second assumption: Role symmetry between substrate and cofactor
A2) For the reaction to occur both reagents must be bound to the enzyme at the same time. In this sense, which one is the co-factor and which one is the substrate is entirely interchangeable. Thus, we could consider that the conversion of $NADP^+$ to NADPH is a reaction catalyzed by G6PD which requires G6P as a cofactor. This would yield a different reaction schematic in 1) but the problem would remain mathematically identical.

Third assumption: Bimolecular binding kinetics between enzyme and cofactors.
A3) Once we have selected which reagent is the substrate and which is the cofactor based on the symmetry assumption in A2, we can assume that the enzyme will be under two possible forms. The form E is the form that is unbound to the cofactor. It is inactive. When the enzyme binds to the cofactor, it becomes activated and is noted as E (E* = E bound to the cofactor). In a well-mixed constant volume system, mass conservation dictates that $[E]_0 = [E] + [E^*]$. Inactive enzymes are assumed to be inert and do not contribute to the enzymatic reaction.*
It ensures that the binding kinetics of the enzyme and cofactor follows a bimolecular kinetics:

$$\frac{d[E^*]}{dt} = k_{on}[E][coF] - k_{off}[E^*] \tag{3.1}$$

Fourth assumption: Michaelis-Menten kinetics
A4) The enzymatic reactions follow a Michaelis-Menten kinetics.

$$\frac{d[Y]}{dt} = \frac{k_{cat}[E^*][X]}{K_M + [X]} \tag{3.2}$$

Where [X] is the concentration of substrate, [Y] is the concentration of the product, and [E] is the active enzyme concentration. The value for [E*] can be obtained by solving eq. 3.1.*

Fifth assumption: Spatial variations of the concentration of species
A5) When the reagents are not perfectly mixed in a stagnant volume, they will experience diffusion and reaction simultaneously. In this case, the reaction equations become more complex as they must include species transport in space. The concentration [X] for example, was previously only dependent on the time t in well mixed conditions. From now on, when we will write the concentration of species [X], we will imply that this variable depends on space and time. [X] -> [X](x,y,z,t). The simpler ordinary differential equations (ODEs) of the well mixed situation become partial differential equations (PDEs) when we include spatial variations. These equations are much more complex to solve. However, we can achieve it relatively easily using finite difference models (FDMs).

Reactions in non-well-mixed stagnant media obey the diffusion-reaction transport equation.

$$\frac{\partial[X]}{\partial t} = D_X \nabla^2[X] + R_X \tag{3.3}$$

Where D_X is the species diffusion constant, R_X is the rate of production of species X at every point in space and time ($R_X(x,y,z,t)$). Finally, ∇ is the differential operator. For example, assuming a Michaelis-

Menten kinetics converting species X into species Y, we get the following equation, in fully developed form:

$$\frac{\partial[Y](x,y,z,t)}{\partial t} = D_Y \nabla^2[Y](x,y,z,t) + \frac{k_{cat}[E^*](x,y,z,t)[X](x,y,z,t)}{K_M + [X](x,y,z,t)} \tag{3.4}$$

While [Y] increases, [X] must necessarily decrease. So there exists another associated diffusion-reaction equation to establish the spatiotemporal distribution of species X.
Before writing it, we observe that in a simple irreversible enzymatic conversion of X into Y, the instantaneous local rate of production of Y equals the local loss in X.

$$R_X = -R_Y; \frac{d[X](x,y,z,t)}{dt} = -\frac{d[Y](x,y,z,t)}{dt} \tag{3.5}$$

The resulting diffusion-reaction equation for species X is thus:

$$\frac{d[X](x,y,z,t)}{dt} = D_X \nabla^2[X](x,y,z,t) - \frac{k_{cat}[E^*](x,y,z,t)[X](x,y,z,t)}{K_M + [X](x,y,z,t)} \tag{3.6}$$

4) Exact model

Following the above arguments and assumptions, one can derive a complete model of diffusion-reaction for all combined species. Each species will be represented by a PDE describing the transport of the species of the form described in eq. 3.3.

4.1 Reaction rates for all substrates, products, cofactors and ions.

Before we establish the transport equations, we observe the following equivalences in the reaction rates of different species:

E1) Every conversion of G6P into 6PGL converts one $NADP^+$ into NADPH. However, every conversion of RZ into RF* converts a NADPH into $NADP^+$. The reaction rates, for all species, can be described as follows according to these rules. All follow a Michaelis-Menten kinetics. The kinetics of Hydrogen ion production is for now omitted as, in first approximation, we neglect the pH dependence of fluorescent signals for small pH variations.

$$R_{G6P} = -R_{6PGL}; R_{RF*} = -R_{RZ}; R_{NADPH} = 2R_{H+} = -R_{NADP+} = R_{G6P} - R_{RF*} \tag{4.1}$$

With, explicitly:

$$R_{G6P} = -R_{6PGL} = -\frac{k_{cat,1}[G6PD^*][G6P]}{K_{M,1} + [G6P]} \tag{4.2}$$

$$R_{RF^*} = -R_{RZ} = \frac{k_{cat,2}[DP*][RZ]}{K_{M,2} + [RZ]} \tag{4.3}$$

$$R_{NADP+} = -\frac{k_{cat,1}[G6PD^*][G6P]}{K_{M,1} + [G6P]} + \frac{k_{cat,2}[DP^*][RZ]}{K_{M,2} + [RZ]} \tag{4.4}$$

$$R_{NADPH} = \frac{k_{cat,1}[G6PD^*][G6P]}{K_{M,1} + [G6P]} - \frac{k_{cat,2}[DP^*][RZ]}{K_{M,2} + [RZ]} \tag{4.5}$$

E2) For enzymes, their activity follows a second order (bimolecular) binding kinetic as described in eq. 3.1. Explicitly, we obtain:

$$R_{G6PD^*} = -R_{G6PD} = k_{on,1}[G6PD][NADP+] - k_{off,1}[G6PD^*] \tag{4.6}$$

$$R_{DP^*} = -R_{DP} = k_{on,2}[DP][NADPH] - k_{off,2}[DP^*] \tag{4.7}$$

Enzymes are exchanged between the active and inactive form during the reaction with $NADP^+$ or NADPH cofactors.

5) Complete Model – Coupled diffusion-reaction equations of all species

The complete coupled PDE model to account for enzymatic conversion in an inhomogeneous fluid volume can now be stated. To do so, we explicitly write, for all 10 species (2 G6PD forms, 2 DP forms, NADPH, $NADP^+$, G6P, 6PGL, RZ, RF*) the diffusion-reaction in eq. 3.3 with the corresponding reaction rates described in equations 4.2 - 4.7. The result is highlighted in table S2 below.

Table S2: Fully-coupled, time-dependent, inhomogeneous diffusion-reaction model for coupled G6PD-Diapharase enzymatic reactions

Equation	Equation number
$\frac{\partial[G6P]}{\partial t} = D_{G6P}\nabla^2[G6P] - \frac{k_{cat,1}[G6PD^*][G6P]}{K_{M,1}+[G6P]}$	(5.1)
$\frac{\partial[6PGL]}{\partial t} = D_{6PGL}\nabla^2[6PGL] + \frac{k_{cat,1}[G6PD^*][G6P]}{K_{M,1}+[G6P]}$	(5.2)
$\frac{\partial[NADP+]}{\partial t} = D_{NADP+}\nabla^2[NADP+] - \frac{k_{cat,1}[G6PD^*][G6P]}{K_{M,1}+[G6P]} + \frac{k_{cat,2}[DP^*][RZ]}{K_{M,2}+[RZ]}$	(5.3)
$\frac{\partial[NADPH]}{\partial t} = D_{NADPH}\nabla^2[NADPH] + \frac{k_{cat,1}[G6PD^*][G6P]}{K_{M,1}+[G6P]} - \frac{k_{cat,2}[DP^*][RZ]}{K_{M,2}+[RZ]}$	(5.4)
$\frac{\partial[RZ]}{\partial t} = D_{RZ}\nabla^2[RZ] - \frac{k_{cat,2}[DP^*][RZ]}{K_{M,2}+[RZ]}$	(5.5)
$\frac{\partial[RF^*]}{\partial t} = D_{RF^*}\nabla^2[RF^*] + \frac{k_{cat,2}[DP^*][RZ]}{K_{M,2}+[RZ]}$	(5.6)
$\frac{\partial[G6PD^*]}{\partial t} = D_{G6PD^*}\nabla^2[G6PD^*] + k_{on,1}[G6PD][NADP+] - k_{off,1}[G6PD^*]$	(5.7)
$\frac{\partial[G6PD]}{\partial t} = D_{G6PD}\nabla^2[G6PD] - k_{on,1}[G6PD][NADP+] + k_{off,1}[G6PD^*]$	(5.8)
$\frac{\partial[DP^*]}{\partial t} = D_{DP^*}\nabla^2[DP^*] + k_{on,2}[G6PD][NADP+] - k_{off,2}[DP^*]$	(5.9)
$\frac{\partial[DP]}{\partial t} = D_{DP}\nabla^2[DP] - k_{on,2}[G6PD][NADP+] + k_{off,2}[DP^*]$	(5.10)

Thus, we have a set of 10 coupled PDEs to solve simultaneously on a 1D domain (a line with no flux (null derivatives) on both sides). As a result, we will have only two independent variables, x and t.

6) Boundary, initial and mass conservation constrains, pseudo steady-state approximations, and initial simplifications.

We can note that 6PGL and RF are not coupled to the other transport equations (they appear only in their respective transport equation) because they are “dead end” products. They are only necessary to account for mass balance. Therefore, we can remove eq. 5.2 and 5.6 from the list, as their values are only deduced from the other equations. To compute RF*, which is the most important result, one can simply use the solution for RZ, once calculated.

Another observation that can be made is that the equations describing G6P depletion (5.1), 6PGL production (5.2), RZ depletion (5.5) and RF* production (5.6) do not reach a steady state until all substrates are converted into products. On the other hand, the number of activated enzymes G6PD* and DP* do reach an equilibrium dependent on the concentration of co-factor NADPH and $NADP^+$. Assuming that these equilibria are quickly achieved compared to the depletion characteristic times of the substrates, one can use a pseudo-steady state approximation and rewrite equations (5.7-5.10) as two steady-state algebraic equations. This has the effect of removing all unknown rate constants from our model and two equations.

With these approximations in hand, a simplified pseudo-steady state model of the reaction can be obtained, as shown in Table S3.

Table S3: Pseudo-steady state reduced two-enzyme kinetics model

Equation	Equation number
$\frac{\partial[G6P]}{\partial t} = D_{G6P}\nabla^2[G6P] - \frac{k_{cat,1}[G6PD^*][G6P]}{K_{M,1}+[G6P]}$	(6.1)
$\frac{\partial[NADP+]}{\partial t} = D_{NADP+}\nabla^2[NADP+] - \frac{k_{cat,1}[G6PD^*][G6P]}{K_{M,1}+[G6P]} + \frac{k_{cat,2}[DP^*][RZ]}{K_{M,2}+[RZ]}$	(6.2)
$\frac{\partial[NADPH]}{\partial t} = D_{NADPH}\nabla^2[NADPH] + \frac{k_{cat,1}[G6PD^*][G6P]}{K_{M,1}+[G6P]} - \frac{k_{cat,2}[DP^*][RZ]}{K_{M,2}+[RZ]}$	(6.3)
$\frac{\partial[RZ]}{\partial t} = D_{RZ}\nabla^2[RZ] - \frac{k_{cat,2}[DP^*][RZ]}{K_{M,2}+[RZ]}$	(6.4)
$[G6PD^*] = [G6PD]_0\frac{[NADP+]}{K_{d,1}+[NADP+]}$	(6.5)*
$[DP^*] = [DP]_0\frac{[NADPH]}{K_{d,2}+[NADPH]}$	(6.6)*
$\frac{\partial[RF^*]}{\partial t} = D_{RF^*}\nabla^2[RF^*] + \frac{k_{cat,2}[DP^*][RZ]}{K_{M,2}+[RZ]}$ (independent, computed from (6.4))	(6.7)

* These binding isotherms are analogous to a Michaelis-Menten binding kinetics. Therefore, K_d can also be called K_M in this case. This means that the data on the Michaelis-Menten constant for $NADP^+$ binding found in the literature (350 µM) can actually be used instead of K_d. This removes two unknowns from our model (NADPH and $NADP^+$ binding constants).

7) Diffusion and reaction parameters

7.1 Diffusion coefficients

We have specified 10 different diffusion coefficients. However, observing that in all cases, substrates are almost identical to products in terms of molecular mass, we can assume that their diffusion rates will not change. Similarly, since enzymes are large molecules and NADPH is a small molecule, we can assume that the activated form of the enzyme will diffuse at the same rate at the inactive form. With these considerations in mind, we only need 5 independent diffusion coefficients to completely describe the species.

Table S4. Diffusion coefficient of the molecules involved in the enzymatic reactions that are included in the mathematical model

Reagent	Diffusion constant	Unit	Reference	Remarks
G6P	534	$\mu m^2.s^{-1}$	[3]	
6PGL	534	$\mu m^2.s^{-1}$		Assumed to be similar to G6P
$NADP^+$	420	$\mu m^2.s^{-1}$	[4]	
NADPH	420	$\mu m^2.s^{-1}$		Assumed to be similar to $NADP^+$
Resazurin	480	$\mu m^2.s^{-1}$	[5]	
Resorufin	480	$\mu m^2.s^{-1}$		Assumed to be similar to resazurin
G6PD	74	$\mu m^2.s^{-1}$	Not found in literature. Calculated using the Stokes-Einstein equation[1]	
G6PD*	74	$\mu m^2.s^{-1}$		Assumed to be similar to G6PD
Diaphorase	74	$\mu m^2.s^{-1}$	[6]	
Diaphorase*	74	$\mu m^2.s^{-1}$		Assumed to be similar to Diaphorase

7.2 Rate and equilibrium constants

The values for the Michaelis-Menten constants K_M [M] and the binding isotherms K_d (equivalent to K_M) [M] were found in the literature. The turnover number K_{cat} [s^{-1}] was calculated as described in section 7.3 from the activity provided by the vendor. Precise intervals were obtained for every one of them, except the Michaelis-Menten constant of Resazurin, for which only a lower bound was obtained [7]. They are all represented in Table S5.

Table S5. Relevant parameters needed to model the enzymatic reactions

Enzyme	Parameter	Short	Value	Unit	Reference
G6PD	K_M G6P	$K_{M,1}$	52	µM	[8]
	K_d $NADP^+$	$K_{d,1}$	7	µM	[8]
	activity	Act_{G6PD}	225	$U.mg^{-1}$	datasheet
	molecular weight	MW	59257	$g.mol^{-1}$	[9]
	$K_{cat(G6PD)}$	$K_{cat,1}$	222.21	s^{-1}	calculated from activity
Diaphorase	K_M resazurin	$K_{M,2}$	out of measurable range, known to be > 34	µM	[7]
	K_d NADPH	$K_{d,2}$	350	µM	[10]
	activity	Act_{DP}	5.6	$U.mg^{-1}$	datasheet
	molecular weight	MW	40000	$g.mol^{-1}$	datasheet
	$K_{cat(diaphorase)}$	$K_{cat,2}$	3.73	s^{-1}	calculated from activity

[1] Stokes-Einstein equation: $D = \frac{k_b T}{6\pi\eta a}$, where D is the diffusion coefficient, K_b the Boltzmann constant, T the temperature, η the viscosity of water, a the effective molecular radius (3.3 nm for G6PD).

7.3 Example of calculation of the turnover number based on enzymatic activity reported by the vendors.

$$K_{cat} = \frac{V_{max}}{[E]_{mol} * 60} \tag{7.1}$$

The activity of the enzyme is provided by the vendor as:

$$Act = \frac{V_{\max}}{m_{enzyme}} \, , which \; leads \; to$$

$$V_{max} = Act * m_{enzyme} \tag{7.2}$$

The mass of the enzyme can be written as:

$$m_{enzyme} = [E]_{gram} * Vol \tag{7.3}$$

The concentration of the enzyme expressed in g/L and in mol/L are linked by the molecular weight:

$$[E]_{gram} = [E]_{mol} * MW \tag{7.4}$$

Inserting equations (7.2), (7.3), (7.4) into (7.1) we obtain:

$$K_{cat} = \frac{V_{max}}{[E]_{mol} * 60} = \frac{Act * [E]_{mol} * MW * Vol}{[E]_{mol} * 60} = \frac{Act * MW * Vol}{60} \tag{7.5}$$

V_{max}: maximum rate of reaction, when the enzyme is saturated with substrate [mol.L^{-1}.min^{-1}]
Act: enzyme activity provided by the vendor and expressed as: $Act = \frac{V_{max}}{m_{prot}}$ [mol.L^{-1}.min^{-1}g^{-1}]
m_{enzyme}: the mass of the enzyme
$[E]_{gram}$: enzyme concentration expressed in g/L
$[E]_{mol}$: enzyme concentration expressed in mol/L
Vol: volume
U: 1U [µmol.min^{-1}], or international unit, is defined as the amount of the enzyme that catalyzes the conversion of one micromole of substrate per minute under the specified conditions of the assay method [11].

8) Implementation using finite difference model

8.1 Pseudo 1D approximation

The characteristic diffusion time for the selected geometric scales with ℓ^2/D in every independent dimension. Knowing that the thickness of the SCM is much smaller than the width, which is smaller than the length, we can approximate that $t_m \sim L^2/D \gg W^2/D \gg H^2/D$ where t_m is the measurement window. With this assumption, a 1D model is sufficiently accurate to capture all the physics of the problem. In extreme cases where reagents are heavier, time scales widthwise could reach the same order of magnitude as time scales lengthwise. The current model does not treat such cases, but a second dimension could easily be added if need be.

8.2 Implementation using Matlab

Numerical simulations of Eqs 5.1-5.10 are completed using Finite Differences (FD) with a second order central FD scheme in space and an explicit first order FD scheme in time. Space is discretized on a uniform grid of size Δx and time steps Δt are defined using two tolerance criterions. First, to correctly capture the physics of the problem we set a tolerance factor on the amount of mass that can react within a time interval Δt. This is to ensure smooth mass changes even when reactions are fast. The second tolerance criterion is a simple upper limit set by the von Neumann stability condition, i.e. the diffusion stability limit. The discretized FD equations read

$$C_{n,i}^{t+\Delta t} = C_{n,i}^{t} + \Delta t \left[D_n \frac{C_{n,i-1}^{t} - 2C_{n,i}^{t} + C_{n,i+1}^{t}}{\Delta x^2} + R_{n,i}^{t} \right]$$

where $C_{n,i}^{t}$ and $R_{n,i}^{t}$ are respectively the concentration and reaction rate at time t and grid node i for the nth specie. Diffusion constants and reaction rates are taken from Tables S4-5. Neumann boundary conditions are set at both ends of the 1D domain and initial concentrations are set by the user. In this study, G6PD is homogeneous throughout the domain and the other solutions are constant by parts with steps widths defined by the spotting diameter such as to mimic experiments. An example of initial concentration values is presented in Table S6. Convergence analyses in space and time and comparison with analytical asymptotic solutions were done to ensure the code is reliable. Simulation speed is highly dependent of reactions speed. Assuming an initial set of concentrations as portrayed in Table S6 with a discretized 1D space of 1000 nodes, simulations for 10 min of physical time takes roughly 120-130s on a single CPU on a laptop. Time steps in this case are largely reaction limited. The FD method was selected for its implementation speed and the non-existence of geometrical complexities for the problem at hand. The code was built in-house from scratch and written using MATLAB R2018a.

Table S6. Initial concentrations example for the simulation of Eqs. 5.1-5.10. Variables that are not shown are set to zero.

Variable	Initial concentration [µM]
[G6P]_0	43460
[$NADP^+$]_0	2173
[RZ]_0	2173
[G6PD]_0	0.012; 0.0188
[DP]_0	388

SI References

1. Guo, T., Patnaik, R., Kuhlmann, K., Rai, A. J. & Sia, S. K. Smartphone dongle for simultaneous measurement of hemoglobin concentration and detection of HIV antibodies. *Lab Chip* **15**, 3514–3520 (2015).
2. Gökçe, O., Mercandetti, C. & Delamarche, E. High-Content Optical Codes for Protecting Rapid Diagnostic Tests from Counterfeiting. *Anal. Chem.* **90**, 7383–7390 (2018).
3. Lucas, L. H., Otto, W. H. & Larive, C. K. The 2D-J-DOSY experiment: Resolving diffusion coefficients in mixtures. *J. Magn. Reson.* **156**, 138–145 (2002).
4. Siritanaratkul, B. *et al.* Transfer of photosynthetic NADP+/NADPH recycling activity to a porous metal oxide for highly specific, electrochemically-driven organic synthesis. *Chem. Sci.* **8**, 4579–4586 (2017).
5. Schilling, E. A., Kamholz, A. E. & Yager, P. Cell lysis and protein extraction in a microfluidic device with detection by a fluorogenic enzyme assay. *Anal. Chem.* **74**, 1798–1804 (2002).
6. Hosoda, S., Nakamura, W. & Hayashi, K. Properties and reaction mechanism of DT diaphorase from rat liver. *J. Biol. Chem.* **249**, 6416–6423 (1974).
7. Catomeris, P. & Thibert, R. J. Study and optimization of the resazurin/diaphorase system. *Microchem. J.* **38**, 390–398 (1988).
8. Wang, X. T., Lam, V. M. S. & Engel, P. C. Marked decrease in specific activity contributes to disease phenotype in two human glucose 6-phosphate dehydrogenase mutants, G6PD(Union) and G6PD(Andalus). *Hum. Mutat.* **26**, 284 (2005).
9. PhosphoSitePlus. Available at: https://www.phosphosite.org/proteinAction?id=4120&showAllSites=true.
10. Chakraborty, S., Sakka, M., Kimura, T. & Sakka, K. Cloning and expression of a Clostridium kluyveri gene responsible for diaphorase activity. *Biosci. Biotechnol. Biochem.* **72**, 735–741 (2008).
11. Labuda, J. *et al.* Terminology of bioanalytical methods (IUPAC Recommendations 2018). *Pure Appl. Chem.* **90**, 1121–1198 (2018).